IIETA International Information and Engineering Technology Association
Advancing the World of Information and Engineering

Annales de Chimie - Science des Matériaux
Vol. 49, No. 3, June, 2025, pp. 291-297
Journal homepage: http://iieta.org/journals/acsm

Enhancing Optical and Structural Properties of Lead-Free Cesium Europium Halide Perovskite Nanocrystals via Carbon Quantum Dots

Hayder Hasan Ali[1,2*], Majid R. Al-Bahrani[1]

[1] Department of Physics, College of Science, University of Thi-Qar, Nasiriyah 64001, Iraq
[2] Department of Science, College of Basic Education, University of Sumer, Nasiriyah 64001, Iraq

Corresponding Author Email: hdoun1992@gmail.com

https://doi.org/10.18280/acsm.490308

Received: 28 April 2025
Revised: 8 June 2025
Accepted: 15 June 2025
Available online: 30 June 2025

Keywords:
lead-free perovskites, carbon quantum dots, europium doping, hot-injection synthesis, photovoltaic applications, perovskite solar cells

ABSTRACT

Despite the exceptional optoelectronic properties of lead-based perovskites, their toxicity remains a critical barrier for commercial applications. This study addresses this challenge by developing non-toxic $CsEuCl_3$ nanocrystals doped with carbon quantum dots (CQDs) to enhance light absorption and stability. Our objectives focus on synthesizing phase-pure $CsEuCl_3$ via hot-injection, optimizing CQD incorporation to reduce bandgap, and characterizing structure-property relationships for photovoltaic use. The results revealed that 3 wt% CQDs incorporation into $CsEuCl_3$ significantly improved light absorption efficiency and reduced the optical bandgap compared to pristine $CsEuCl_3$ and other CQDs concentrations.

1. INTRODUCTION

Over the past few years, perovskite halides with ABX_3 lattices, where A represents a monovalent organic cation (e.g., $CH_3NH_3^+$) or inorganic cation (e.g., Cs^+ or Rb^+), B represents a divalent metal ion (e.g., Sn^{2+}, Pb^{2+}, Mn^{2+}, or Ge^{2+}), and X is a halogen (e.g., F, Cl, Br, or I), have gained significant research interest due to their promising photovoltaic applications [1], including light-emitting diodes (LEDs) [2, 3], solar cells [4, 5], catalysis [6], and photodetectors [7]. Recently, a large number of all-inorganic metal halide perovskites, especially cesium-based perovskites ($CsBX_3$), have gained great interest due to their remarkable thermal stability as well as their interesting optoelectronic properties [8, 9].

Many divalent metal ions, such as Pb^{2+}, Sn^{2+}, and Mn^{2+}, have been frequently used as B-site cations in $CsBX_3$ perovskites, especially lead (Pb^{2+})-based halide perovskites in the past few years, the high potential of using perovskite $CsPbX_3$ nanoparticles as an active layer in perovskite solar cells has been demonstrated [10].

Lead exposure primarily causes irreversible damage to the central nervous system (e.g., cognitive impairment in children) and renal dysfunction, as Pb^{2+} accumulates in bones and soft tissues [11]. These severe health risks necessitate lead-free alternatives.

Consequently, the pursuit of lead-free perovskite nanocrystals exhibiting minimal or negligible toxicity, robust photovoltaic performance, and superior environmental stability has gained significant momentum. Owing to the extensive structural and compositional versatility within the perovskite family, numerous lead-free halide perovskite nanocrystals have been successfully synthesized and comprehensively characterized in recent years. So far, Sn(II) [12, 13], Sn(IV) [14], Sb(III) [15], Bi(III) [16], Cu(I) [17], Ag(I) [18], Na(I) [19], Yb(II) [20], and Eu(II) [21, 22] have been explored as potential replacements for lead. Some of these materials exhibit decent optoelectronic performance comparable to their lead-based counterparts. These encouraging results in the exploration of lead-free perovskite nanocrystals show promising potential for breakthroughs in the fabrication of novel optoelectronic devices.

Europium (Eu) is an effective light-sensing element in perovskite materials [23]. Divalent Eu^{2+} (117 pm) substitutes Pb^{2+} (119 pm) in the perovskite lattice, increasing the tolerance factor ($t \approx 0.9$) closer to the ideal cubic phase ($t = 1$), thereby enhancing structural stability [22, 24]. However, bulk europium halide perovskite crystals synthesized via solid-state methods face limitations in controlling their homogeneity and shape. Colloidal synthesis of rare earth halide perovskites can provide improved homogeneity and tunable shapes. Recently, there have been studies on the synthesis of nanocrystals of cesium bromide and cesium bromide mixed with Eu^{2+}; however, pure europium halide perovskites still present challenges [25, 26].

There are several reported methods for synthesizing perovskite nanocrystals. However, the most widely used and popular method is the hot-injection method, rapid injection of Cs-oleate at 200°C, followed by ice quenching (≤ 5°C), ensures supersaturation, inducing instantaneous nucleation. This kinetic control limits crystal growth to the nanoscale (10–30 nm) and favors cubic/rectangular morphologies, critical for tunable bandgap and charge transport [27].

Recent studies have demonstrated the potential of carbon-

based nanomaterials, including carbon nanotubes and graphene, in modifying the light-absorbing layer to suppress non-radiative recombination losses [28]. Nevertheless, significant challenges remain in simultaneously enhancing the photoelectric performance and environmental stability of these devices [29, 30]. Among various nanomaterials, carbon quantum dots (CQDs) have garnered considerable research interest due to their exceptional optical properties and tunable electronic characteristics. The optical properties of CQDs are of particular interest, as they exhibit the unusual trait of excitation-dependent emission [31].

In this work, we demonstrate the solution-phase synthesis of cesium-europium halide perovskite nanocrystals ($CsEuCl_3$) and investigate their structural and optical properties. The structural characteristics were analyzed using X-ray diffraction (XRD), field-emission scanning electron microscopy (FESEM), and transmission electron microscopy (TEM), while the optical properties were examined via UV-Vis spectroscopy. Furthermore, we incorporated carbon quantum dots (CQDs) into the $CsEuCl_3$ nanocrystals at varying weight ratios to form nanocomposites and evaluated the influence of CQDs on optical absorbance and energy bandgap. This study presents a promising lead-free alternative to halide perovskites for potential applications in perovskite solar cells and optoelectronic devices.

2. MATERIALS AND METHODS

2.1 Materials

Europium(III) chloride ($EuCl_3$, 99.99%) and cesium carbonate (Cs_2CO_3, 99.9%) were purchased from Fisher Chemicals. 1-Octadecene (ODE, 90%), oleic acid (OA, 90%), oleylamine (OlAm, 99.9%), octanoic acid (OcAc, 99%), trioctylphosphine (TOP, 97%), 1-butyl-1-methylpyridinium chloride, hexane (anhydrous, 95%), carbon quantum dots (CQDs, 0.5 mg/mL in water), and toluene (anhydrous, 99.8%) were obtained from Sigma-Aldrich. All chemicals were used as received without further purification.

2.2 Preparation of Cs-oleate solution

A mixture of cesium carbonate (Cs_2CO_3, 0.5 g), 1-octadecene (ODE, 16 mL), and oleic acid (OA, 1 mL) was loaded into a 50 mL three-neck flask. The reaction mixture was vigorously stirred and degassed under vacuum at 120°C for 1 hour. Subsequently, the system was purged with nitrogen (N_2), and the temperature was gradually increased to 150°C under continuous N_2 flow to facilitate the complete reaction between Cs_2CO_3 and OA. The resulting Cs-oleate solution solidified upon cooling to room temperature and was reheated to 100°C prior to injection to ensure complete dissolution of the precipitate.

2.3 Synthesis of $CsEuCl_3$ nanocrystals via hot-injection method

The synthesis of $CsEuCl_3$ nanocrystals (NCs) was performed under inert atmosphere conditions using standard air-free techniques. In a nitrogen-filled glovebox, europium(III) chloride ($EuCl_3$, 0.54 g) and 1-octadecene (ODE, 10 mL) were loaded into a 50-mL three-neck flask equipped with a condenser. The reaction vessel was subsequently removed from the glovebox, and the mixture was subjected to degassing at 140°C for 2 hours under vacuum to ensure complete removal of oxygen and moisture.

Following this pretreatment, the system was purged with nitrogen and maintained under positive N_2 pressure. Oleylamine (OlAm) and oleic acid (OA, 1 mL each) were then injected into the reaction mixture, resulting in the formation of a pale yellow solution within 30 minutes. The temperature was subsequently elevated to 200°C under continuous nitrogen flow.

At this stage, 1 mL of preheated (100°C) Cs-oleate precursor solution was rapidly injected into the reaction mixture. After precisely 1 minute of reaction time, immediate quenching was achieved by immersion in an ice bath. The crude product was then subjected to purification through sequential centrifugation (3000 rpm, 10 minutes) and washing cycles. Specifically, the supernatant was decanted after initial centrifugation, and the precipitate was redispersed in hexane (10 mL). This washing procedure was repeated with an additional 4 mL of hexane to ensure complete removal of reaction byproducts. The purified $CsEuCl_3$ NCs were finally dispersed in anhydrous hexane and stored at 4°C for subsequent characterization.

2.4 Synthesis of $CsEuCl_3$:CQDs nanocomposites

The nanocomposites were prepared through a facile and cost-effective solution-phase method employing commercially available solvents. In a typical synthesis, 4 mL of $CsEuCl_3$ nanocrystal solution was introduced into a 25 mL three-neck flask under continuous N_2 purge at 120°C. Subsequently, carbon quantum dots (CQDs) were incorporated at varying mass ratios (1, 3, and 5 wt%), with rigorous stirring maintained for 60 minutes to ensure homogeneous dispersion and effective composite formation. The resulting $CsEuCl_3$:CQDs nanocomposite solutions were subsequently stored at 4°C in sealed vials to prevent degradation prior to characterization (Figure 1).

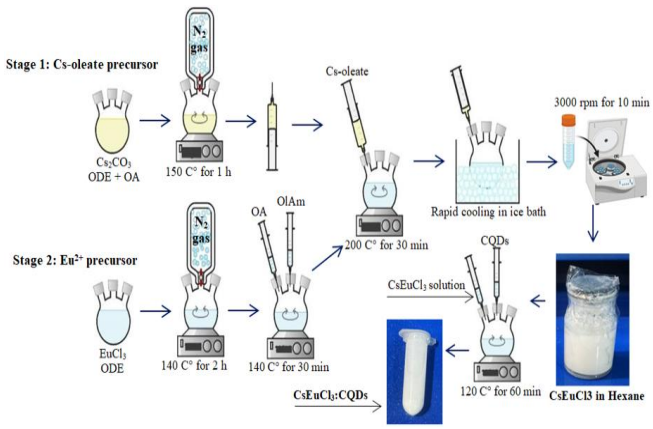

Figure 1. Schematic of $CsEuCl_3$:CQDs synthesis

2.5 Deposition $CsEuCl_3$ NCs and $CsEuCl_3$:CQDs thin films

Under an inert atmosphere of N_2, thin films were prepared by adding 1-butyl-1-methylpyridinium chloride (0.05 mmol), OlAc (0.5 mL), and OlAm (0.5 mL) to a 25 mL three-neck flask. The solution was stirred at 100°C on a magnetic stirrer inside a glove box until 1-butyl-1-methylpyridinium chloride

was completely dissolved. Subsequently, the $CsEuCl_3$ NCs or $CsEuCl_3$:CQDs solution was mixed with the above solution and stirred on a magnetic stirrer at 100°C for 2 h. The spin-coating method was then employed to deposit the $CsEuCl_3$ NCs or $CsEuCl_3$:CQDs at 2000 rpm for 30 s on glass, followed by drying at 100°C.

3. RESULT AND DISCUSSION

3.1 Structural characterization

The four FE-SEM images analyzed reveal distinct crystal structures of perovskite compounds synthesized via the hot-injection method. Figure 2 displays pure $CsEuCl_3$ perovskite crystals, characterized by a compact morphology and uniform grain distribution.

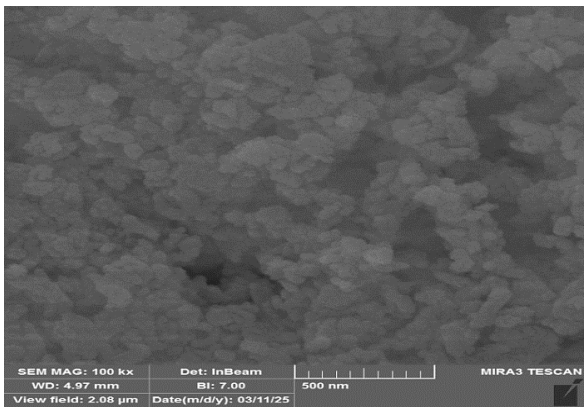

Figure 2. FE-EM characterization of the perovskite nanocrystal structures Pure $CsEuCl_3$

Figure 3, incorporating 1% CQDs, exhibits minor compositional modifications, suggesting that CQD integration may enhance optical properties, particularly absorbance and bandgap tuning.

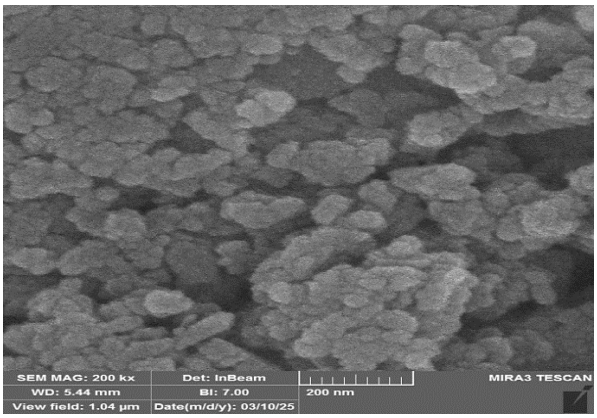

Figure 3. FE-EM characterization of the perovskite nanocrystal structures Pure $CsEuCl_3$ with 1 wt% CQDs

A more ordered structure with reduced intergranular spacing is observed in Figure 4 (with 3% CQDs), indicative of significantly improved absorbance and a narrower bandgap. This enhancement stems from optimized perovskite-CQD interactions, which promote efficient photon absorption and charge carrier transport, rendering this composition highly suitable for perovskite solar cell applications.

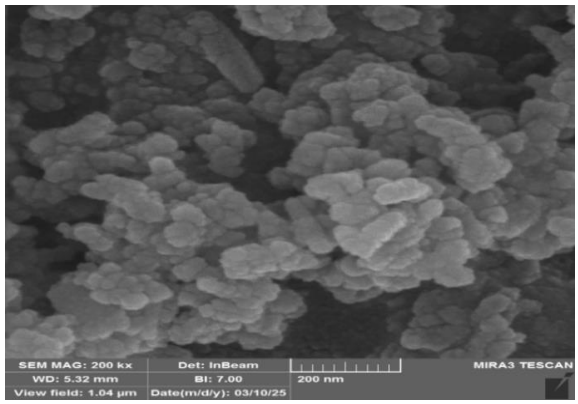

Figure 4. FE-EM characterization of the perovskite nanocrystal structures Pure $CsEuCl_3$ with 3 wt% CQDs

In contrast, Figure 5 demonstrates the formation of large, heterogeneous aggregates, which likely impede charge transport and introduce structural defects despite the high nanoparticle density. These findings suggest that perovskites can serve as effective active absorber layers in solar cells, with the 3% CQDs formulation offering an optimal balance between optical performance and electronic properties.

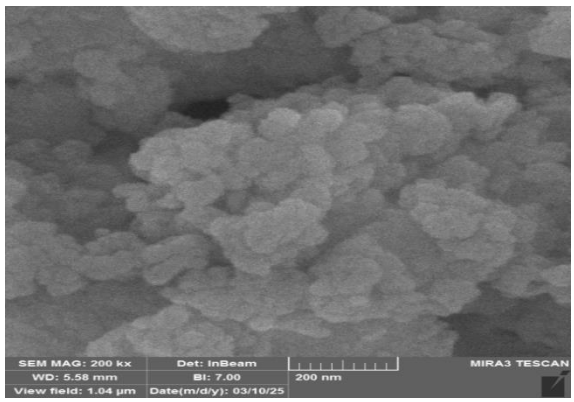

Figure 5. FE-EM characterization of the perovskite nanocrystal structures Pure $CsEuCl_3$ with 5 wt% CQDs

TEM images from this study demonstrate a clear evolution in the nanostructure of $CsEuCl_3$ perovskite crystals upon the addition of carbon quantum dots (CQDs). Figure 6 shows $CsEuCl_3$ perovskite crystals with cubic and rectangular morphologies exhibiting distinct size distribution variations. The cubic morphology reflects the optimal crystal structure of the ABX_3 system with cubic symmetry, indicating sample purity and the absence of major defects, consistent with previous studies reporting such crystal structures in metal halide nanostructures.

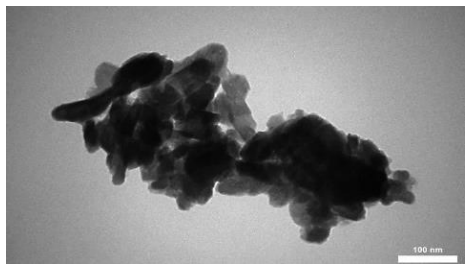

Figure 6. TEM characterization of the perovskite nanocrystal structures Pure $CsEuCl_3$

With the incorporation of 1% CQDs (Figure 7), small nanoparticles (< 10 nm) appear distributed sparsely on the perovskite surface while maintaining the compound's basic structure, potentially leading to modest optical property enhancements.

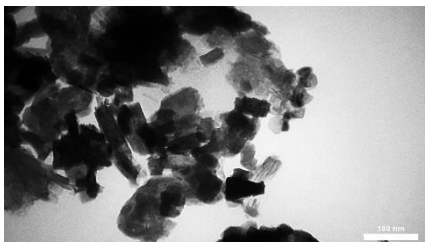

Figure 7. TEM characterization of the perovskite nanocrystal structures $CsEuCl_3$ with 1 wt% CQDs

Figure 8 (3% CQDs) demonstrates optimal quantum dot distribution, where homogeneous dispersion within the perovskite matrix forms effective crystal interfaces, resulting in improved absorbance and reduced energy gap (Eg). This CQD:$CsEuCl_3$ interaction enhances light absorption by extending into the infrared region and improves charge transport through conductive nanopathway formation.

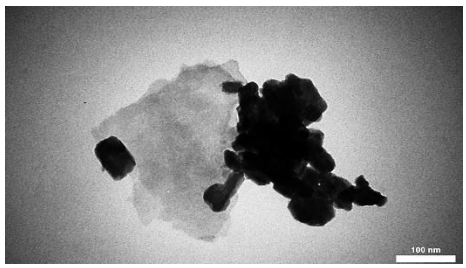

Figure 8. TEM characterization of the perovskite nanocrystal structures $CsEuCl_3$ with 3 wt% CQDs

In contrast, Figure 9 (5% CQDs) reveals significant quantum dot clustering, causing perovskite crystal structure distortions and increased defect density. These morphological changes impede charge transport, reduce electron-hole separation efficiency, and initiate gradual property degradation. The results establish that 3% CQDs incorporation represents the optimal concentration, achieving both homogeneous quantum dot distribution and preservation of $CsEuCl_3$ optical and electrical properties.

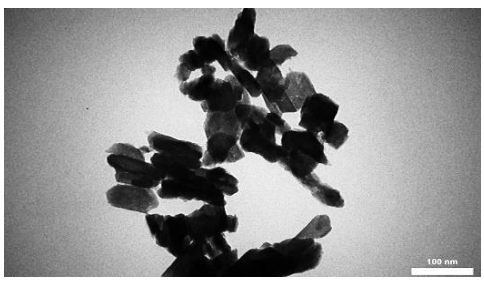

Figure 9. TEM characterization of the perovskite nanocrystal structures $CsEuCl_3$ with 5 wt% CQDs

To investigate whether the addition of CQDs would alter the crystal structure of $CsEuCl_3$, the XRD patterns of pure $CsEuCl_3$ film and $CsEuCl_3$ films with different proportions of CQDs are shown in Figure 10. The XRD results were found to be in good agreement with the standard pattern of $CsEuCl_3$ NCs. The lattice constants of the (111), (112), (101), (211), and (222) crystal planes were determined to be 26.57, 32.74, 37.63, 51.11, and 54.83 Å, respectively, based on the tetragonal phase (See Table 1).

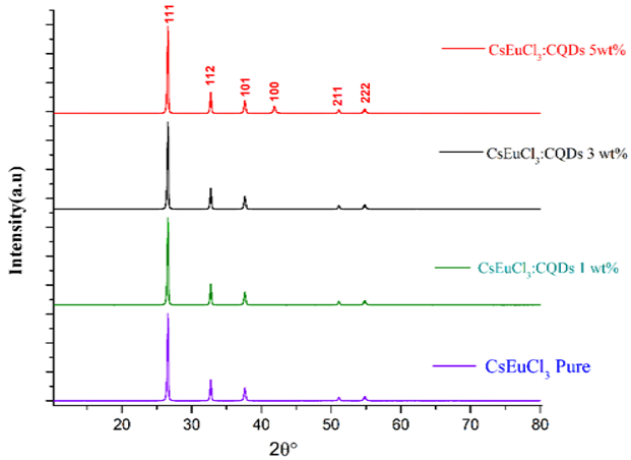

Figure 10. XRD patterns of pure $CsEuCl_3$ film and $CsEuCl_3$ films with different concentrations of CQDs additives

When CQDs were added to $CsEuCl_3$ perovskite crystals at concentrations of 1 and 3%, and X-ray diffraction (XRD) analysis was performed, no new peaks appeared. This is attributed to the insufficient concentration of CQDs to exceed the critical threshold required for structural modification. However, the appearance of the (100) diffraction peak at angle 41.88° in the 5% CQDs sample, but not in its lower concentration counterparts, reflects the occurrence of a critical structural change at this ratio, where the quantum dot concentration exceeds the structural effect threshold (~4.2%) to form an interconnected network, causing sufficient lattice strain to distort the Eu-Cl bond angles, leading to a decrease in absorbance and an increase in the optical energy gap.

3.2 Optical characterization

3.2.1 Absorbance

The incorporation of carbon quantum dots (CQDs) into lead-free $CsEuCl_3$ perovskite nanocrystals results in significant modifications to their optical absorption properties and bandgap energies, as demonstrated by UV-Vis spectroscopy (Figure 11) and Tauc plot analysis (Figure 12). A significant improvement in absorption was observed in the wavelength range of 400–850 nm compared to the pure thin film. This enhancement can be attributed to the role of CQDs as charge transport mediators within the perovskite structure, suppressing non-radiative recombination and increasing the effective surface area of the $CsEuCl_3$ NCs. These effects collectively improve the efficiency of light absorption and electron-hole pair generation. However, a decrease in absorbance was observed for the thin film with 5 wt% CQDs. This reduction may be due to the clustering of quantum dots at higher concentrations, leading to non-uniform dispersion, hindered charge transport, and the introduction of defects in the perovskite structure (as confirmed by TEM). Additionally, the clustered CQDs may act as light-blocking agents, preventing photons from reaching the $CsEuCl_3$ NCs and thereby reducing absorption.

Table 1. Characteristics of $CsEuCl_3$ perovskite crystals, peak positions, FWHM, grain size, and chemical elements with reference codes

Peaks Positions (2θ)	FWHM(β)	Grain Size (nm)	Chemical Element	hkl	Reference Code
26.57	0.20546	39.71	Cs	111	00-018-0326
32.74	0.23399	35.37	Cl	112	01-072-1642
37.63	0.30132	27.84	Eu	101	00-038-0928
41.88	0.37274	22.81	C	100	01-080-0004
51.11	0.28936	30.42	Cl	211	01-072-1642
54.83	0.39806	22.47	Cs	222	00-018-0326

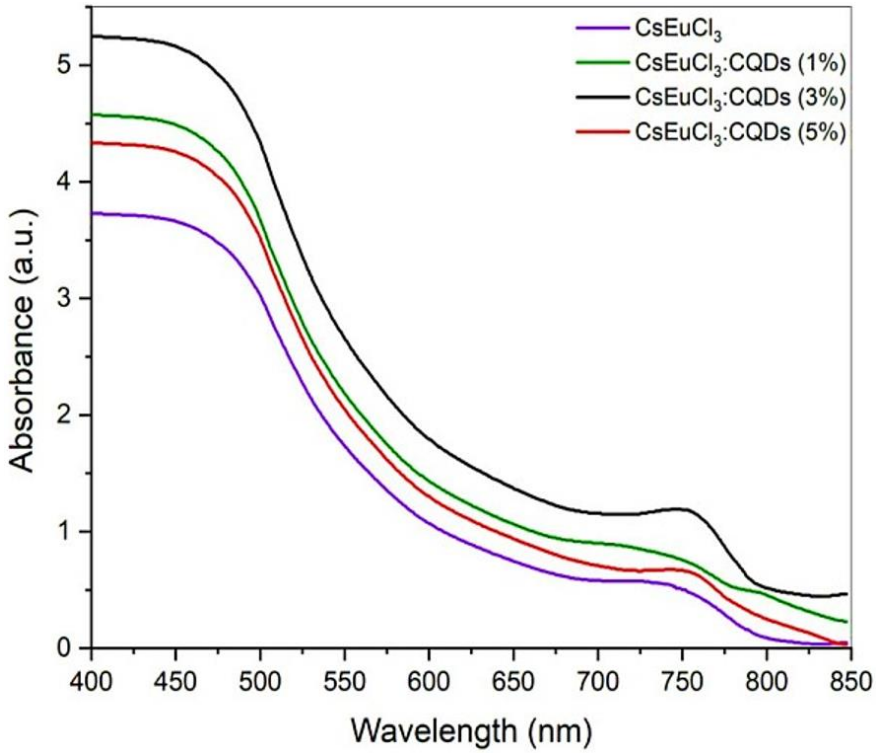

Figure 11. Absorption spectra of pure $CsEuCl_3$ NCs films and $CsEuCl_3$ films containing different proportions of CQDs

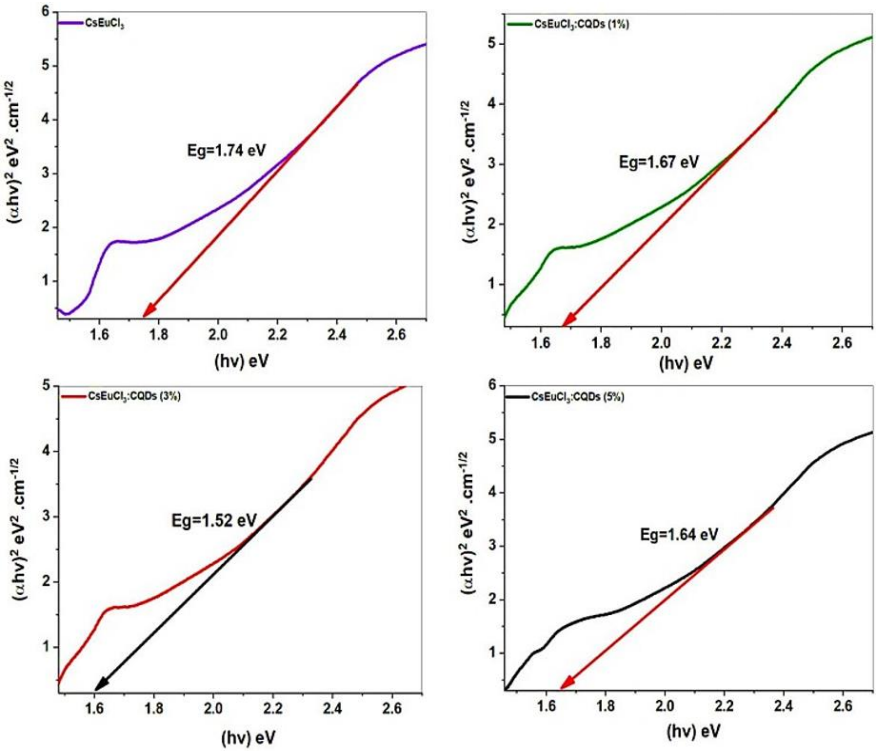

Figure 12. Tauc plot of optical band gaps for perovskite thin films

3.2.2 Optical energy gap

Figure 12 shows that the optical bandgap decreases from 1.67 eV to 1.52 eV upon the addition of 1% and 3% CQDs, respectively. The incorporation of CQDs may modify the electronic structure of perovskites by introducing intermediate energy states or shifting the conduction and valence band edges. This reduces the energy required for electronic transitions, enhances charge carrier mobility, and suppresses non-radiative recombination, thereby facilitating the generation of electron-hole pairs. However, when the CQDs concentration increases to 5%, the quantum dots tend to cluster rather than disperse uniformly. This clustering induces significant lattice strain or distortion, increasing the energy required for electronic transitions and, consequently, the bandgap. Materials with band gaps in this range are well-suited for absorbing higher-energy photons (visible light), making them ideal for use as light-absorbing layers in solar cells. The reduction in the optical bandgap with the addition of 1% and 3% CQDs is highly beneficial for solar cell applications, as it aligns well with the solar spectrum and enhances light absorption efficiency. In contrast, the increase in the optical bandgap with the addition of 5% CQDs is less favorable for solar cell performance.

4. CONCLUSIONS

In summary, we synthesized, developed, and characterized a lead-free $CsEuCl_3$:CQDs perovskite composite with enhanced optoelectronic properties for solar cell applications. The incorporation of 3% CQDs was found to be optimal, significantly improving light absorption, reducing the optical bandgap, and enhancing charge carrier dynamics. These results underscore the potential of CQDs-modified $CsEuCl_3$ as a viable and environmentally friendly alternative to lead-based perovskites in photovoltaic devices. Future work will explore encapsulation techniques for long-term stability and integration into full solar cell devices to evaluate PCE under AM1.5 conditions.

ACKNOWLEDGMENT

This work was supported by the Department of Physics, College of Science, University of Thi-Qar, Iraq, in partial fulfillment of the requirements for the Ph.D. graduation.

REFERENCES

[1] Green, M.A., Ho-Baillie, A., Snaith, H.J. (2014). The emergence of perovskite solar cells. Nature Photonics, 8(7): 506-514. https://doi.org/10.1038/nphoton.2014.134

[2] Liu, X.K., Xu, W., Bai, S., Jin, Y., Wang, J., Friend, R.H., Gao, F. (2021). Metal halide perovskites for light-emitting diodes. Nature Materials, 20(1): 10-21. https://doi.org/10.1038/s41563-020-0784-7

[3] Xiao, Z., Kerner, R.A., Zhao, L., Tran, N.L., Lee, K.M., Koh, T.W., Scholes, G.D., Rand, B.P. (2017) Efficient perovskite light-emitting diodes featuring nanometre-sized crystallites. Nature Photonics, 11(2): 108-115. https://doi.org/10.1038/nphoton.2016.269

[4] Isikgor, F.H., Zhumagali, S., T. Merino, L.V., De Bastiani, M., McCulloch, I., De Wolf, S. (2023). Molecular engineering of contact interfaces for high-performance perovskite solar cells. Nature Reviews Materials, 8(2): 89-108. https://doi.org/10.1038/s41578-022-00503-3

[5] Rong, Y., Hu, Y., Mei, A., Tan, H., Saidaminov, M. I., Seok, S.I., McGehee, M.D., Sargent, E.H., Han, H. (2018). Challenges for commercializing perovskite solar cells. Science, 361(6408): eaat8235. https://doi.org/10.1126/science.aat8235

[6] Hwang, J., Rao, R. R., Giordano, L., Katayama, Y., Yu, Y., Shao-Horn, Y. (2017). Perovskites in catalysis and electrocatalysis. Science, 358(6364): 751-756. https://doi.org/10.1126/science.aam7092

[7] Dou, L., Yang, Y., You, J., Hong, Z., et al. (2014). Solution-processed hybrid perovskite photodetectors with high detectivity. Nature Communications, 5(1): 5404. https://doi.org/10.1038/ncomms6404

[8] Moschou, G., Koliogiorgos, A., Galanakis, I. (2018). Electronic properties of Cs-Based halide perovskites: An Ab initio study. Physica Status Solidi (a), 215(17): 1700941. https://doi.org/10.1002/pssa.201700941

[9] Yan, W., Sun, Y., Zhao, X., Yang, W., et al. (2024). Carrier mobilities and band alignments of inorganic perovskites of $CsBX_3$. Journal of Materials Chemistry C, 12(28): 10733-10741. https://doi.org/10.1039/D4TC01939C

[10] Swarnkar, A., Marshall, A.R., Sanehira, E.M., Chernomordik, B.D., et al. (2016). Quantum dot-induced phase stabilization of α-$CsPbI_3$ perovskite for high-efficiency photovoltaics. Science, 354(6308): 92-95. https://doi.org/10.1126/science.aag2700

[11] Flora, G., Gupta, D., Tiwari, A. (2012). Toxicity of lead: A review with recent updates. Interdisciplinary Toxicology, 5(2): 47. https://doi.org/10.2478/v10102-012-0009-2

[12] Ali, H.H. (2023). Preparation and characterization of ZnO NWs/graphene nanocomposite as an effective photoanode electrode for improving the performance of the dye-sensitized solar cells. University of Thi-Qar Journal of Science, 10(1): 11-15.

[13] Lin, R., Xiao, K., Qin, Z., Han, Q., et al. (2019). Monolithic all-perovskite tandem solar cells with 24.8% efficiency exploiting comproportionation to suppress Sn (ii) oxidation in precursor ink. Nature Energy, 4(10): 864-873. https://doi.org/10.1038/s41560-019-0466-3

[14] Nakamura, T., Yakumaru, S., Truong, M.A., Kim, K., et al. (2020). Sn (IV)-free tin perovskite films realized by in situ Sn (0) nanoparticle treatment of the precursor solution. Nature Communications, 11(1): 3008. https://doi.org/10.1038/s41467-024-51361-2

[15] Noculak, A., Morad, V., McCall, K.M., Yakunin, S., et al. (2020). Bright blue and green luminescence of Sb (III) in double perovskite Cs2MInCl6 (M= Na, K) matrices. Chemistry of Materials, 32(12): 5118-5124. https://doi.org/10.1021/acs.chemmater.0c01004

[16] Lyu, M., Yun, J.H., Cai, M., Jiao, Y., et al. (2016). Organic–inorganic bismuth (III)-based material: A lead-free, air-stable and solution-processable light-absorber beyond organolead perovskites. Nano Research, 9(3): 692-702.

[17] Zhao, X.G., Yang, D., Sun, Y., Li, T., et al. (2017). Cu-In halide perovskite solar absorbers. Journal of the American Chemical Society, 139(19): 6718-6725. https://doi.org/10.1021/jacs.7b02120

[18] Lim, E., Kim, Y.J., Kim, J.H., Ryu, T., et al. (2014). NO oxidation activity of Ag-doped perovskite catalysts. Journal of Catalysis, 319: 182-193. https://doi.org/10.1016/j.jcat.2014.09.007

[19] Retuerto, M., Pascual, L., Calle-Vallejo, F., Ferrer, P., et al. (2019). Na-doped ruthenium perovskite electrocatalysts with improved oxygen evolution activity and durability in acidic media. Nature Communications, 10(1): 2041. https://doi.org/10.1038/s41467-019-09791-w

[20] Moon, B.J., Kim, S.J., Lee, S., Lee, A., et al. (2019). Rare-earth-element-ytterbium-substituted lead-free inorganic perovskite nanocrystals for optoelectronic applications. Advanced Materials, 31(33): 1901716. https://doi.org/10.1002/adma.201901716

[21] Ali, H.H. (2023). Multi-Wall carbon nanotubes with NiO and pt as counter electrodes for DSSC applications. University of Thi-Qar journal of science, 10(2): 141-145. https://doi.org/10.32792/utq/utjsci/v10i2.1124

[22] Kunkel, N., Meijerink, A., Springborg, M., Kohlmann, H. (2014). Eu (ii) luminescence in the perovskite host lattices $KMgH_3$, $NaMgH_3$ and mixed crystals $LiBa_xSr_{1-x}H_3$. Journal of Materials Chemistry C, 2(24): 4799-4804. https://doi.org/10.1039/C4TC00644E

[23] Lefevre, G., Herfurth, A., Kohlmann, H., Sayede, A., et al. (2018). Electron-phonon coupling in luminescent europium-doped hydride perovskites studied by luminescence spectroscopy, inelastic neutron scattering, and first-principles calculations. The Journal of Physical Chemistry C, 122(19): 10501-10509. https://doi.org/10.1021/acs.jpcc.8b01011

[24] Swarnkar, A., Mir, W.J., Nag, A. (2018). Can B-site doping or alloying improve thermal-and phase-stability of all-inorganic $CsPbX_3$ (X= Cl, Br, I) perovskites? ACS Energy Letters, 3(2): 286-289. https://doi.org/10.1021/acsenergylett.7b01197

[25] Alam, F., Wegner, K.D., Pouget, S., Amidani, L., et al. (2019). Eu^{2+}: A suitable substituent for Pb^{2+} in $CsPbX_3$ perovskite nanocrystals? The Journal of chemical physics, 151(23). https://doi.org/10.1063/1.5126473

[26] Yang, Z., Jiang, Z., Liu, X., Zhou, X., et al. (2019). Bright blue light-emitting doped cesium bromide nanocrystals: Alternatives of lead-free perovskite nanocrystals for white LEDs. Advanced Optical Materials, 7(10): 1900108.

[27] Vighnesh, K., Wang, S., Liu, H., Rogach, A.L. (2022). Hot-injection synthesis protocol for green-emitting cesium lead bromide perovskite nanocrystals. ACS Nano, 16(12): 19618-19625.https://doi.org/10.1021/acsnano.2c11689

[28] Zhang, R., Chen, Y., Xiong, J., Liu, X. (2018). Synergistic carbon-based hole transporting layers for efficient and stable perovskite solar cells. Journal of Materials Science, 53(6): 4507-4514. https://doi.org/10.1007/s10853-017-1876-x

[29] Ferguson, V., Silva, S.R.P., Zhang, W. (2019). Carbon materials in perovskite solar cells: prospects and future challenges. Energy & Environmental Materials, 2(2): 107-118. https://doi.org/10.1002/eem2.12035

[30] He, R., Huang, X., Chee, M., Hao, F., Dong, P. (2019). Carbon-based perovskite solar cells: From single-junction to modules. Carbon Energy, 1(1): 109-123. https://doi.org/10.1002/cey2.11

[31] Mintz, K.J., Zhou, Y., Leblanc, R.M. (2019). Recent development of carbon quantum dots regarding their optical properties, photoluminescence mechanism, and core structure. Nanoscale, 11(11): 4634-4652. https://doi.org/10.1039/C8NR10059D